In Vitro Hydrolytic Surface Degradation of Poly(glycolic acid): Role of the Surface Segregated Amorphous Region in the Induction Period of Bulk Erosion

Joo-Woon Lee and Joseph A. Gardella, Jr.*

Department of Chemistry, State University of New York at Buffalo, Buffalo, New York 14260-3000

Received December 29, 2000

ABSTRACT: The in vitro hydrolytic degradation of thin (ca. 100 μm) films of poly(glycolic acid) (PGA) has been studied, focusing on the kinetics of degradation of the near surface phases. The emphasis of this work is to describe the nature of the initial "induction" period of hydrolysis of biodegradable polyesters, where water absorption is initiating into the surface phase and weight loss is not detectable. The kinetics of surface degradation are shown to be related to the enrichment of amorphous PGA in the surface phases. This study presents results from both surface and bulk phase characterization of short-term (<10 h) exposures of PGA to buffered systems at physiological temperatures. The role of pH of the external buffer medium in influencing the rate of PGA hydrolytic surface degradation is quantified using time-of-flight secondary ion mass spectrometry (ToF SIMS), using previously developed methods to determine the rates of production of oligomeric reaction products. Scanning electron microscopy (SEM) studies show changes in surface morphology over these exposure periods. X-ray photoelectron spectroscopy (XPS) data are given to support the chemistry of the process. Finally, DSC data on the changes in bulk crystallinity and weight loss studies confirm the nature of the early stages of the reaction. Results show that the relative hydrolytic surface degradation rates in pH 4.0 and 10.0 buffer media are approximately 3 times faster than that in pH 7.4 buffer, but the change in crystallinity at pH 4.0 is less than that at pH 10.0. SEM results show the emergence of increased surface crystallinity at the more extended exposure times in this study (6 h). No detectable weight loss is reported for these exposures. A model of the reaction chemistry of the induction period is presented which involves the initial rapid, pH-dependent hydrolysis of surface segregated amorphous PGA, with little overall weight loss as water absorption is still reaching equilibrium in the reaction zone. These results indicate that the reaction kinetics during the initial induction period could lead to rapid drug delivery from the surface with little release of monomeric glycolic acid upon initiation of reaction.

Introduction

The compelling need to develop biodegradable polymers[1] for drug delivery and tissue engineering has prompted the development of analytical approaches with emphasis on both surface and bulk characterization. Defining the role of surface vs bulk erosion processes is important since the surface is the direct contact region that is expected to dictate at least the initial in vivo performance; further, the surface properties cannot be always predicted from observation of the bulk properties. This is often due to a specific molecular or oligomeric orientation or composition at the surface or surface specific chemical reactions.

It is known that a bulk erosion mechanism[2−5] based on both in vivo and in vitro observations is responsible for the main degradation of biodegradable polyesters: random chain scission on the linkage of ester bonds in the polymer backbone proceeds homogeneously throughout the matrix. The bulk degradation pathway[2,4,5] has three major features in the polymer erosion profile (Figure 1): (1) incubation, without changes in weight and molecular weight (MW), which reflects the interval required for water penetration into the polymer matrix, (2) induction, with a decrease in MW and a rapid increase in the degree of matrix hydration followed by saturation, and (3) onset of polymer erosion (weight loss)

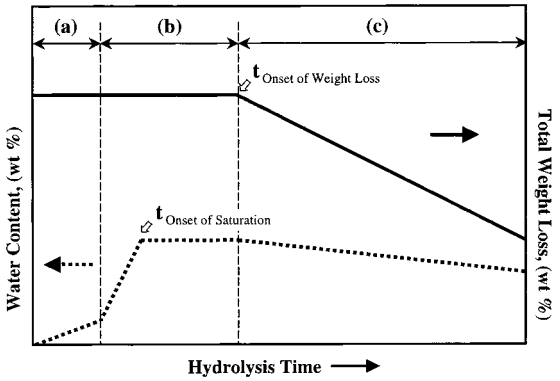

Figure 1. Descriptive hydrolytic bulk erosion profile for semicrystalline biodegradable polyesters: (a) incubation, (b) induction, (c) polymer erosion.

and any changes in the rate of chain scission. Recently, however, it has been reported that large devices of biodegradable polyesters degrade via a heterogeneous mechanism;[6−8] i.e., the degradation proceeds more rapidly in the center than at the surface. This is attributed to the autocatalytic action of the carboxylic acid end groups of degradation products that are trapped in the matrix. While studies of the surface of biodegradable polymeric materials[9−19] have provided chemical composition, structural information, or images of the morphological changes for visualization during hydrolytic degradation, there have been few reports[16,19] of quantitative results about the surface degradation

* To whom correspondence should be addressed. Tel (716) 645-6800, ext 2111; Fax (716) 645-5994; E-mail gardella@acsu.buffalo.edu.

10.1021/ma0022351 CCC: $20.00
Published on Web 05/03/2001

behavior. Thus, surface studies of the reactivity of biodegradable polymers have an essential value, not only for a fundamental understanding of hydrolytic surface degradation kinetics but also toward the design and formulation of new biodegradable polymers and their fabrication into new devices.

Poly(glycolic acid) (PGA)[20−25] is a highly crystalline, hydrophilic, linear aliphatic polyester that is the simplest biodegradable poly(α-hydroxy acid) and has been shown to undergo hydrolytic degradation both in vitro and in vivo.[2,26,27] It has a high melting point and a very low solubility in most common organic solvents with the exception being hexafluoro-2-propanol. Because of its biocompatibility and biodegradability, PGA and its copolymers have been studied for potential dental,[28,29] drug delivery,[30−32] and orthopaedic[33] applications since its first commercial application as absorbable sutures under the trade name Dexon by the American Cyanamid Corp. in the 1970s.[34−36] Although PGA and its copolymers have been of research interest for decades, most of the work has been bulk phase studies. These have involved the use of techniques which analyze the bulk properties[37−40] such as time for total degradation, drug release profiles, extent of water absorption, total weight loss, crystallinity, tensile strength, thermal properties, and molecular weight as a function of treatment time. In addition to this, the hydrolytic bulk degradation kinetics of PGA are not completely understood, and the effect of local pH on them is still unclear.[2,41−44] There are contradictory results about the influence of the pH of the external medium on the rate of bulk degradation. Acceleration of the degradation rates at low[42] pH as well as high[43,44] pHs has been reported, yet other results[2,41] showed pH-independent hydrolysis in vitro. Reed and Gilding[41] reported that the insensitivity of pH on hydrolytic degradation kinetics was due to the combined effects of hydrophobic/hydrophilic balance and crystallinity in the experiments performed with PGA and its copolymers with poly(lactic acid) (PLA) and poly(lactic-*co*-glycolic acid) (PLGA). The extent of water hydration was thought to determine the rate of degradation; this is supported by the fact that amorphous PLGA[42] was degraded faster than semicrystalline PGA, and a lower rate of degradation was observed for stereoregular poly(L-lactic acid) (PLLA) relative to amorphous poly(DL-lactic acid) (PDLLA).[5] Following an accelerated degradation testing of these polymer nonwovens, however, Dauner et al.[45] showed that no significant effect from the crystallinity was detected. Li et al.[46] reported that degradation-induced morphology changes of large size amorphous PDLLA devices were observed during degradation with the partial crystallization of degradation byproducts or residues. Hence, the degradation of PGA, PLA, and their copolymers may be significantly influenced by many factors such as morphology and crystallinity of the material and formulation, besides the structure, molecular weight, and composition of the polymers. The amorphous fraction, which is assumed to be surface segregated from atomic force microscopy (AFM) studies[17−19] on a series of biodegradable polymers, may also play a role in both bulk and surface degradation. Therefore, the roles of morphology and crystallinity on surface and bulk reaction kinetics have yet to be fully explained.

The first surface characterization of PGA was reported by Davies et al.[9−13] using SIMS and X-ray photoelectron spectroscopy (XPS). The SIMS data provided a detailed molecular fingerprint of PGA surface structure, and a good correlation was observed between the theoretical and experimental elemental/chemical state information from XPS. However, the highest mass in the positive SIMS spectra reported in those works was 300 Da, due to the use of a quadrupole mass analyzer. Other techniques[15−19] such as scanning electron microscopy (SEM), AFM, and surface plasmon resonance (SPR) have made it possible to characterize surface morphologies at subnanometer and even atomic resolution. These surface microscopy techniques, however, do not provide chemical composition and structural information. In our laboratory we have also studied the surface reaction chemistry of degradation.[47−50] XPS was not capable of detecting hydrolysis occurring at the surface of PGA due to the intrinsic detection limits[47] of changes in elemental concentrations as a result of the treatment. Although XPS was unable to detect slight changes at the surfaces in a PGA hydrolysis study, in previous papers[48−50] we have reported[48] the detection of the hydrolytic degradation process at the surface of PGA using time-of-flight secondary ion mass spectrometry (ToF SIMS). Those results were the first attempt in high mass range (over 1000 Da) to detect and quantify the hydrolytic degradation at the surface of PGA. Identifying the surface reaction products using ToF SIMS has been also demonstrated[49] as a powerful technique for screening new biodegradable polymers. Recently, we have reported[50] the ToF SIMS determination of hydrolytic surface degradation kinetics of thick (1 mm) plates of PGA under various pH conditions. In particular, results[50] showed acceleration of the degradation rate at the surface in sodium hydroxide adjusted pH 10.0 ISOTON II solution with a reduced buffer capacity (β) from the original pH 7.4 buffer and deceleration observed in potassium carbonate−potassium borate−potassium hydroxide buffer solution (pH 10.0) and potassium hydrogen phthalate buffer solution (pH 4.0).

In our previous studies of PGA surface reaction kinetics,[50] however, we did not control the crystallinity of the thick samples nor study the degradation rate of crystalline vs amorphous regions. In addition, it is known[50] that boric acid, a Lewis acid, generated in potassium carbonate−potassium borate−potassium hydroxide buffer (pH 10.0) during the hydrolysis treatment of PGA samples could have a retardation effect on the hydrolytic surface degradation.

In the present work, by fabricating a thinner sample with reproducible crystallinity and using other buffer systems without borate as a chemical component, we investigate the role of the surface segregated amorphous fraction influencing surface and bulk degradation at different buffered pHs during the induction period of bulk erosion processes with increasing hydrolysis time. Physical, chemical, and morphological studies of the PGA films were carried out using SEM, XPS, and ToF SIMS for the surface determination and differential scanning calorimetry (DSC) for the bulk thermal properties and weight loss studies for the confirmation of induction period.

Experimental Section

Materials. High molecular weight PGA (mol wt > 300 000) used in this study was supplied by Dr. Peter Jarrett of Davis & Geck Division of American Cyanamid Co. (One Casper, St. Danbury, CT). ISOTON II (pH 7.4 at 25 °C), a physiological

Table 1. Saline Buffer Solutions used in Hydrolysis Treatment

saline solution	composition	buffer capacity (β)	ionic strength (I or μ)
ISOTON II (pH 7.4): physiological electrolyte buffer	NaCl (7.93 g/L) $Na_2EDTA{\cdot}2H_2O$ (0.38 g/L) KCl (0.40 g/L) NaH_2PO_4 (0.19 g/L) NaH_2PO_4 (1.85 g/L) NaF (0.30 g/L)	NA	
sodium carbonate buffer (pH 10.0)	$NaHCO_3$ (0.025 M) Na_2CO_3 (0.025 M)	0.030	0.10
sodium biphthalate buffer (pH 4.0)	$NaO_2CC_6H_4CO_2H$ (0.05 M)	0.016	0.05

electrolyte buffer solution, was purchased from Coulter Diagnostics (a division of Coulter Electronics, Inc., Hialeah, FL). Sodium biphthalate buffer solution (pH 4.0 at 25 °C) and sodium carbonate buffer solution (pH 10.0 at 25 °C) were prepared with buffer concentrates (DILUT-IT) purchased from T. J. Baker Inc. Reagent grade *n*-hexane (Fisher Scientific) was used for surface cleaning as received without further purification.

Transparent Sample Preparation. Transparent 100 μm PGA samples were prepared by melt-casting 1 mm thick PGA disks[47−50] between aluminum foil sheets precleaned using *n*-hexane. Before preparing the transparent PGA samples, PGA disks were cut to small pieces and ultrasonically cleaned in *n*-hexane for 2 min. A piece of PGA disk was pressed at above 200 °C for a few seconds and cooled in air, and then the aluminum foil sheets were peeled off for the PGA samples which were transparent. These samples were ultrasonically cleaned again in *n*-hexane for 2 min to remove any impurities that may have been transferred from the aluminum foil sheets. Typical contamination might have resulted in signals from residual Al_2O_3 (e.g., $^{27}Al^+$) or signals from low mass organic contaminants, which would not be present above 300 Da. The extent of surface contamination was equal or below.

Hydrolysis Treatment. All hydrolysis treatments were performed in various buffer solutions for times ranging from 1 to 6 h at 37.0 ± 0.2 °C using a constant-temperature bath (Fisher Circulator model 73). The experiments were conducted in neutral buffer solution (ISOTON II, pH 7.4), sodium carbonate buffer solution (pH 10.0), and sodium biphthalate buffer solution (pH 4.0) in order to regulate the autocatalytic effect of carboxylic acid end groups in the bulk generated during hydrolysis treatment. Detailed information about the composition of the saline buffers is listed in Table 1. Transparent PGA samples were immersed in 24 mL of aqueous treatment solution prefilled in 25 mL vials, and then the whole vial was placed in the isothermal water bath, which was already at the hydrolysis temperature prior to the sample introduction. After the allotted times, PGA samples were removed from the treatment solution in vials and dried in a vacuum oven at ambient temperature at least for 24 h before being analyzed. The pH values of the buffers were monitored after the attempted hydrolysis of PGA using a Digital ionalyzer, model 501, of Orion Research, Inc. (Cambridge, MA). No significant change in pH value was observed in all hydrolysis conditions (0.02−0.05 units).

Bulk Determination. (1) Total Weight Loss Determination. At each preset hydrolysis time, the hydrolyzed samples were taken and weighed after blotting the surface water with tissue. This was defined as the wet weight and includes the amount of free water in the matrix, the amount of bound water associated with the sample, and the dry weight of the hydrolyzed sample. Dry weights were determined after complete drying of the hydrolyzed samples under vacuum for over 24 h. The total weight loss of the hydrolyzed samples was calculated on the basis of the difference of dry weights before and after hydrolysis treatment within the experimental error (±0.1 wt %) using a microbalance (Mettler AE 100). Water contents were based on the dry weights of the hydrolyzed samples.

(2) DSC. Measurements of the heat of fusion (ΔH_f) and melting temperature (T_m) as thermal bulk properties were performed with a Perkin-Elmer 7-series differential scanning calorimeter calibrated with pure indium. All the samples were placed in an aluminum pan, which were scanned from 5 to 240 °C with a scan rate of 10 °C/min. Nitrogen was used as a sweeping gas. All the DSC thermograms were obtained from the first heating cycle. The T_m was taken as the temperature corresponding to the maximum in the endothermic peak, and the ΔH_f was taken as the area under the same peak. The crystallization temperature (T_c) and heat of crystallization (ΔH_c) for the exothermic peak were also taken in the same manner. For the percent crystallinity calculation, ΔH_f was ratioed with the theoretical 100% crystalline $\Delta H_f°$ (191.25 J/g).[51]

Surface Determination. (1) SEM. Samples were vacuum-coated with graphite to make a conducting layer at the surface. Surface morphological changes of the hydrolyzed PGA samples were examined using Hitachi S-4000 and S-800 scanning electron microscopes at 20 kV electron beam radiation.

(2) XPS. The fractions of each oxygen between two functionalities (*O*−C═O/O−C═*O*) were analyzed using a Physical Electronic/PHI 5300 X-ray photoelectron spectrometer operated at 300 W (15 kV and 20 mA). Mg Kα radiation (1253.6 eV) and a pass energy of 89.45 eV for survey as well as 17.9 eV for high-resolution acquisition were used for the angle-dependent acquisitions at a 20° takeoff angle. Curve fitting was performed for each oxygen fractions using AugerScan software (RBD Enterprises, Suite 201, Bend, OR).

(3) ToF SIMS. ToF SIMS analysis was performed using a Physical Electronics 7200 time-of-flight secondary ion mass spectrometer equipped with a cesium ion gun and a channel plate detector. The primary ion gun was operated at 8 keV for all experiments. The static mode was used in all acquisitions with primary ion current of 0.3 pA. The pulse width of primary ion current was 1.0 ns. The extractor was operated in the positive ion mode. The total ion dosage in each spectral acquisition was no more than 1×10^{11} ions/cm^2. An electron neutralizer was operated during all spectral acquisitions in pulsed mode at low electron energy with a target current under 1 mA for charge compensation. The pressure of the main chamber was kept between 10^{-8} and 10^{-10} Torr for each analysis. A time resolution of 1.25 ns per step was used for good signal-to-noise ratio at high mass to charge (m/z) range. The spectra were analyzed using the data reduction software, Physical Electronics TOFPak. Analysis of the surface molecular weight and distribution was performed using Googly software.[52]

Results and Discussion

In our previous work,[47−50] all experiments were carried out with 1 mm thick PGA disks. During all hydrolysis experiment with the 1 mm disks no change in color was observed during the hydrolysis, and no account of crystallinity changes was made. In the present study, however, various physical changes are observed for the transparent 100 μm PGA samples during the hydrolysis treatments. Upon exposure to the treatment solutions, all samples change from visibly transparent to opaque even after 1 h exposure, and they become much more brittle and fragile with increasing

Table 2. Water Contents (wt %) of PGA Films

	hydrolysis condition at 37 °C		
time (h)	ISOTON II (pH 7.4)	carbonate buffer (pH 10.0)	biphthalate buffer (pH 4.0)
2	2.8 ± 0.4	3.0 ± 0.2	2.9 ± 0.3
4	3.5 ± 0.1	3.4 ± 0.3	3.9 ± 0.2
6	3.6 ± 0.2	3.8 ± 0.1	3.9 ± 0.2

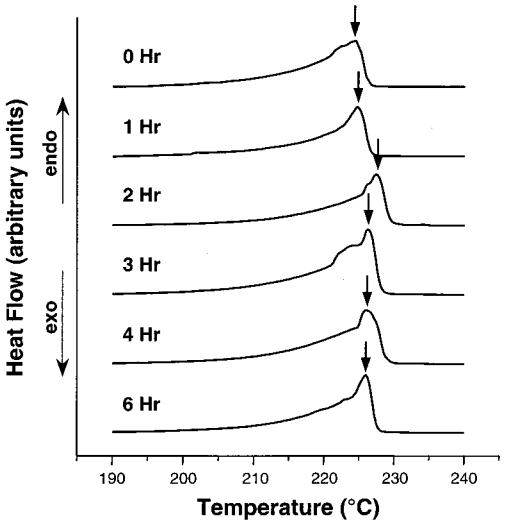

Figure 2. Effect of hydrolysis time on the DSC melting curves of PGA films in pH 10.0 buffer medium.

hydrolysis time. The transparent state indicates the polymer has relatively more amorphous regions in a given polymer system. We propose that the thinner samples in the present DSC study would represent the bulk thermal properties relatively closer to the eroding zone[53] of a layer device or morphology.

Bulk Characteristics. The degradation of PGA involves chain scissions of ester bond linkages in the polymer backbone by hydrolytic attack of water molecules. The degree of hydration in the vicinity of the hydrolytically labile ester bonds will determine the rate of degradation for the samples and may be different for each of three different pH buffers used in the present study. Within a short exposure treatment of up to 6 h, however, no significant change in water content (3−4 wt %) is observed under all conditions regardless of the external pH buffer medium and hydrolysis time (Table 2). Furthermore, there is no change in net dry weight loss. These observations support the proposal that little immediate release of degradation products into the external pH buffer is occurring due to the homogeneous bulk degradation[2,4,5] in PGA. Therefore, it is concluded in this study that the lack of change in total weight is responsible for the characteristic induction period of PGA erosion profile (Figure 1).

On the other hand, it is expected during the induction period that there will be some degree of changes in bulk thermal properties such as heat of fusion (ΔH_f) and melting temperature (T_m) due to potential phase changes associated with water absorption. Thus, in the present study DSC analyses have been done to examine and quantify the changes in crystalline phase composition with respect to hydrolysis time in buffers at the various pHs. Figure 2 shows the effect of hydrolysis time on the DSC melting curves of PGA in pH 10 buffer solution. All samples show a very pronounced endothermic melting transition. The shape of the melting peak and the value of T_m vary with respect to the increase in hydrolysis time. This is evidence for a change in molecular weight during the characteristic induction period. All of thermal data are summarized in Table 3, and the changes in degree of crystallinity in the three different pH buffer media are plotted as a function of hydrolysis time in Figure 3. Crystallinities gradually increase with increasing hydrolysis time; the extent of change is the greatest in pH 10.0 sodium carbonate buffer followed by that in pH 4.0 sodium biphthalate buffer. These results support the hypothesis that the rate of change in the degree of bulk crystallinity is sensitive to the pH of the buffer medium.

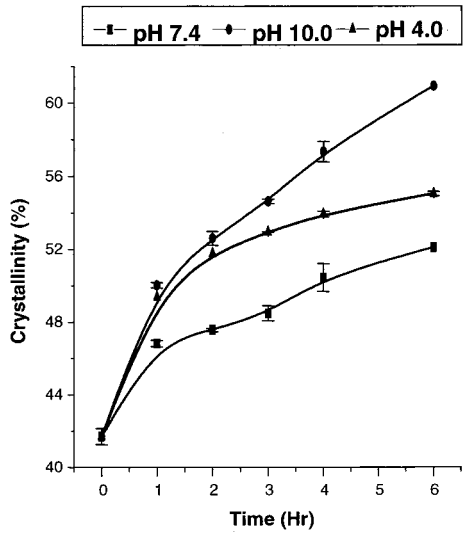

Figure 3. PGA crystallinity change as a function of hydrolysis time in different pH buffer media.

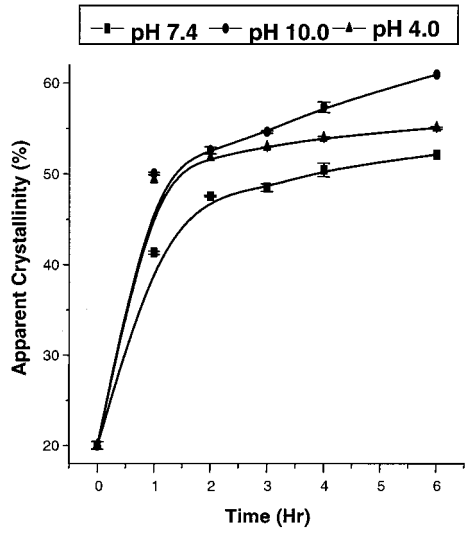

Figure 4. PGA apparent crystallinity change as a function of hydrolysis time in different pH buffer media.

As seen in Table 3, the PGA sample hydrolyzed for 1 h in pH 7.4 ISOTON II buffer solution gives an exothermic crystallization enthalpy (ΔH_c) similar to that of the untreated transparent PGA sample. This is the only treatment that retains this crystallization phenomenon among the samples hydrolyzed in various conditions. Contrary to the endothermic melting enthalpy (ΔH_f), ΔH_c results from the crystallization of polymer, which suggests that the amorphous structure is reorienting into a crystalline form during the DSC heat scan before it melts. So, the presence *or* the absence of ΔH_c will depend on the relative amount of amorphous

Table 3. Effect of Hydrolysis Conditions on PGA Bulk Thermal Properties

hydrolysis condition		thermal properties				
solution	time (h)	T_m (°C)	ΔH_f (J/g)	crystallinity[a] (%)	T_c (°C)	ΔH_c[b] (J/g)
none	0	224.3	79.8	41.7	75.8	−41.5
	1	224.3	89.6	46.8	66.9	−10.5
	2	226.3	91.0	47.6		
ISOTON II: pH 7.4	3	225.8	92.7	48.5		
	4	224.9	96.5	50.4		
	6	224.5	99.6	52.1		
	1	225.3	95.7	50.0		
	2	226.9	100.6	52.6		
carbonate buffer: pH 10.0	3	226.1	104.5	54.6		
	4	225.7	109.7	57.3		
	6	225.3	116.5	60.9		
	1	223.2	94.4	49.4		
	2	224.7	99.0	51.8		
biphthalate buffer: pH 4.0	3	224.2	101.3	53.0		
	4	223.9	103.1	53.9		
	6	224.1	105.3	55.0		

[a] Percent crystallinity for the samples is calculated from $(\Delta H_f/\Delta H_f°) \times 100$ (see text). [b] Negative value represents exothermic characteristics.

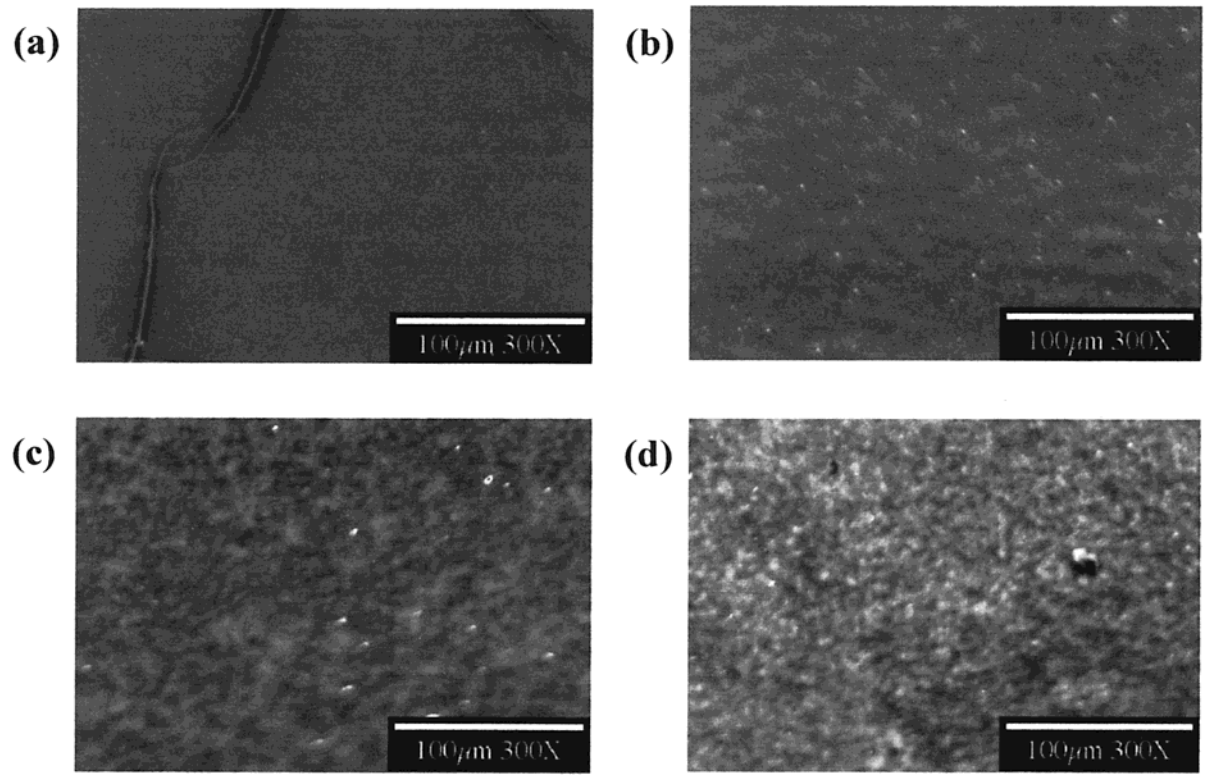

Figure 5. SEM photomicrographs of PGA films hydrolyzed in pH 10.0 buffer medium at 37 °C: (a) 0 h, (b) 1 h, (c) 3 h, (d) 6 h.

phase present in the polymer system. We defined an "apparent crystallinity" by evaluating the difference between the endothermic melting (ΔH_f) and the exothermic crystallization (ΔH_c) enthalpies using the following assumptions: (1) a polymer would give ΔH_c if it has more than a critical amount of amorphous phase, and (2) the difference ($\Delta H_f - \Delta H_c$) would correspond to the amount of original crystallinity. The apparent crystallinities are plotted in Figure 4 as a function of hydrolysis time in each pH buffer. A sudden increase is observed during the first 1 h of treatment in all pH buffer media, and there is a greater difference between neutral and acidic/basic buffers at the 1 h point. This relatively greater difference at 1 h can support the hypothesis that the initial stage of biodegradation of PGA at pH 7.4 ISOTON II buffer is relatively slower than those at other buffered pHs.

Surface Characteristics. To compare the surface erosion process to the above bulk phase studies, SEM photomicrographs were measured for all samples. With increasing hydrolysis time in various buffers, the increase in roughness of the surface is observed. The greatest change in morphology is at the basic buffered pH 10.0 in Figure 5. However, it is difficult to quantitatively assess the degree of morphological change through routine SEM study as a surface technique.

In general, hydrolytic chain scission of ester bonds involves the bond cleavage of acyl−oxygen linkages and the oxygen insertion from water by nucleophilic attack of water molecules to form alcohol and carboxylic acid end groups. A relative increase in the concentration of oxygen functionality (*O*−C═O) is expected as a result of hydrolytic degradation. In an attempt to investigate the increased amounts of oxygen functionality (*O*−

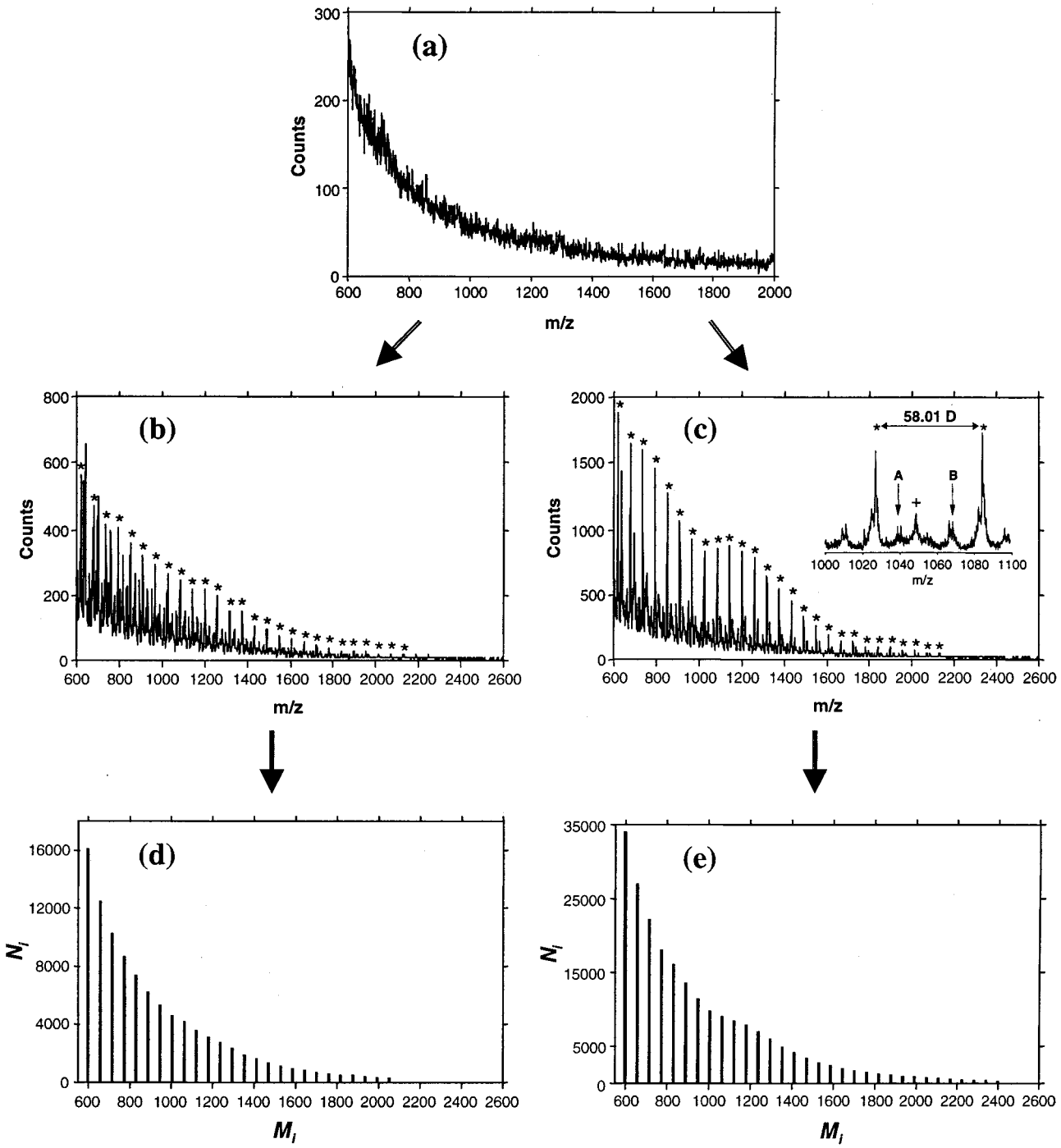

Figure 6. Positive ToF SIMS spectra (a, b, and c) of PGA films before and after hydrolysis treatment in pH 7.4 buffered condition at 37 °C and comparison (d and e) of the corresponding molecular weight distribution (MWD) functions of hydrolysis products, where the star-marks represent the most intense secondary ion distribution: (a) 0 h, (b) 2 h, (c) 6 h, (d) MWD for 2 h, (e) MWD for 6 h.

C═O), an XPS study has been carried out at a 20° takeoff angle using a curve-fitting method for the oxygen 1s line. As a result of the treatment in pH 7.4 ISOTON II buffer, small amounts of sodium and chlorine are detected at the surfaces of the PGA samples. The concentrations are less than 2 atomic % so no adjustments were made in the treatment procedure. No foreign elements are detected adsorbed at the surface treated in both pH 10.0 sodium carbonate and pH 4.0 sodium biphthalate buffers. (Typical detection limits would be 0.25% atomic concentration.) The relative ratio (*O*−C═O/O−C═*O*) between two oxygen functionalities remains unchanged within the error limits of the curve-fitting experiment (±5%) as a result of the hydrolysis. This result, therefore, confirms our previous results[47] that routine XPS study is unable to detect hydrolysis at the surface of PGA samples, and it does not have sufficient detection limits to detect changes at the surface.

In the ToF SIMS spectra, ions from polymer chain fragments are normally observed for both untreated PGA thick[48−50] disks and thin films with an exponential decrease in intensities as *m*/*z* increases (Figure 6a). Very little except a noisy background can be observed in the *m*/*z* range above 600 Da; this is likely due to the entanglement of the long chain polymer molecules,

Table 4. Structural Assignments and Mass Formulas for Positive ToF SIMS Molecular Ion Peak Families within a Set of Ion Peak Patterns

	Possible Chemical Structure	M_i
*	$H\text{-}[OCH_2CO]_{\mathbf{n}}\text{-}OH\text{---}(Na)^+$	
A	$[[OCH_2CO]_{\mathbf{n}}\text{-}OCH_2]\text{---}(Na)^+$	$\mathbf{n} \times M_{mon}$ (58D) + H_2O
+	$H\text{-}[OCH_2CO]_{\mathbf{n}}\text{-}ONa\text{---}(Na)^+$	
B	$CH_3CO\text{-}[OCH_2CO]_{\mathbf{n}}\text{-}OH\text{---}(Na)^+$	
*	$H\text{-}[OCH_2CO]_{\mathbf{n+1}}\text{-}OH\text{---}(Na)^+$	

which mediates against desorption without multiple bond breaking events. Upon exposure to the treatment solution, however, the chain lengths of PGA are gradually shortened due to the result of hydrolytic degradation, so the degradation-generated oligomers become smaller and less entangled enough to readily desorb from the PGA surface as secondary ions. It has been the hypothesis of the previous work[48−50] that the distribution of peak intensities observed in the high mass range reflects the distribution of PGA hydrolysis products at the surface of the material. The positive ToF SIMS spectra of Figure 6b,c show oligomeric molecular ion distributions of the hydrolysis products of PGA obtained from pH 7.4 buffered condition at 37 °C for 2 and 6 h, respectively, where the star mark represents the most intense secondary ion distribution. The spacing between consecutive most intense peaks is equal to the repeat unit (M_{mon}) of PGA (M_{mon} = 58.01 amu) from which PGA can be identified, and there are three peaks observed within the spacing as shown in the inset of Figure 6c. This general pattern was observed with various polyesters and polyanhydrides.[49] In Table 4, the star-marked most intense peak represents sodium cationized PGA oligomer ion $(nM_{mon} + H_2O + Na)^+$ as the intact molecule of the hydrolytic degradation product, where the sodium ion comes from the buffer treatment solution and participates in the ionization process as a cationization agent. The cross-marked peak assigned to $(nM_{mon} + OH + 2Na)^+$ is 22 Da greater than the star-marked one with the same repeat number. This indicates one sodium ion replaces one proton in the star-marked PGA oligomer ion. It can be concluded that the star- and cross-marked peaks have arisen from the desorption process of the intact PGA hydrolysis products. Peaks labeled A and B as assigned in Table 4 can be produced by chain fragmentation from the hydrolysis products with longer chain lengths during the ToF SIMS experiment. The same oligomeric ion peak patterns are observed consistently between other consecutive peaks in the spectrum and also observed with the same manner in both pH 10.0 sodium carbonate and pH 4.0 sodium biphthalate buffer solutions.

To extract MW information from the molecular weight distribution (MWD) in ToF SIMS spectra, the intensities of the four peaks with the same repeat number (n) are integrated together to represent the total intensity (N_i, $i = n$) for the particular PGA oligomer ($M_i = nM_{mon} + H_2O$) over the range from 600 Da to the last detectable peak as seen in Figure 6d,e. This database is subsequently analyzed using the conventional statistical averaging definitions for the number-average (M_n) and weight-average (M_w) molecular weights and the polydispersity index (PI).

$$M_n = \sum N_i M_i / \sum N_i \quad (1)$$

$$M_w = \sum N_i M_i^2 / \sum N_i M_i \quad (2)$$

$$PI = M_w / M_n \quad (3)$$

This represents two changes from our previous practice,[48−50] where only the most intense star-marked molecular ion peak, $(nM_{mon} + H_2O + Na)^+$, was counted as representative of oligomer intensity, and only a fixed mass range (e.g., 600−2000 Da) was chosen in all data analyses for the quantification of the molecular weight distribution. We increased the mass range studied in the present work because most of molecular ion peaks in ToF SIMS are detectable beyond 2000 Da with the increase in hydrolysis time. In addition, the precision in data reduction is improved by including all four peaks if all peaks are related to the hydrolysis products. (Details of ToF SIMS quantitation studies will be reported in a separate paper.[54]) The same approach is applied for all of hydrolysis treatments in the two different pH buffer media in the present work.

The results of statistical averaging calculations of the integration are shown in Table 5, and the change in M_n is plotted as a function of hydrolysis time in Figure 7. The decrease in M_n of intact hydrolysis products produced at the surface is observed from 2 or 3 h hydrolysis time after the initial increase. As for the initial increase in MW, the reason for this new phenomenon is believed

Table 5. Molecular Weight Characterization Results for PGA Hydrolysis Products at the Surface

	ISOTON II (pH 7.4)		carbonate buffer (pH 10.0)		biphthalate buffer (pH 4.0)	
time (h)	M_n	PI	M_n	PI	M_n	PI
1	879.2	1.11	940.0	1.14	872.8	1.11
2	931.3	1.14	958.5	1.14	895.4	1.12
3	958.4	1.16	947.6	1.13	898.4	1.12
4	954.3	1.16	936.3	1.14	887.7	1.10
6	947.0	1.14	920.0	1.12	867.6	1.11

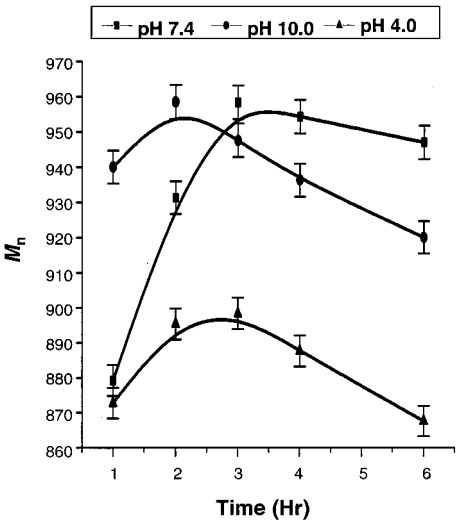

Figure 7. Change in M_n in different pH buffer media as a function of hydrolysis time.

Scheme 1

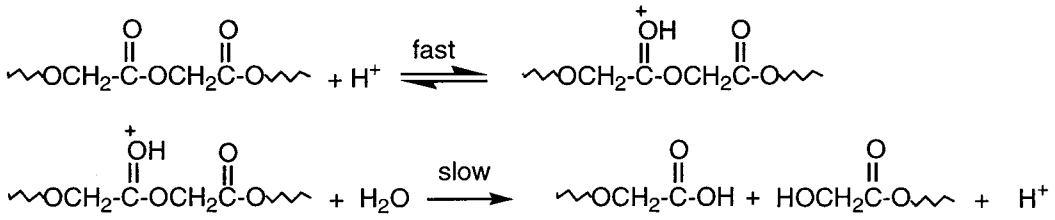

Table 6. Hydrolytic Degradation Kinetics Results at the Surface of PGA in Various Buffers

treatment buffer	pH	rate constant (h^{-1})	R^2
ISOTON II	7.4	2.67×10^{-4}	0.999
sodium carbonate	10.0	7.01×10^{-4}	0.995
sodium biphthalate	4.0	8.49×10^{-4}	0.999

to be preferential degradation of the surface segregated amorphous phase. This hypothesis can be supported by the comparison of the crystallinity and apparent crystallinity of thick plates previously studied (1 mm: 44.4/44.4%) vs the transparent thin films used in this study (100 μm: 41.7/20.0%). This shows a significantly larger amorphous fraction in the thin films. The previous results from thick PGA plates show a gradual decrease in MW as hydrolysis time increases. The segregated amorphous fraction might also be due to the low molecular weight fraction[55,56] of PGA resulting from the melt-casting fabrication.

From the hydrolysis time which shows decreases in M_n, the kinetic expression of PGA hydrolytic degradation at the surface can be established according to the hydrolysis mechanism of ester linkages. Equation 4 is used for the noncatalytic chain scission[50,57] in pH 7.4 ISOTON II buffer solution:

$$\ln[(DP - 1)/DP] = -k't + \ln[(DP_0 - 1)/DP_0] \quad (4)$$

where $k' = k[H_2O]$, and DP and DP_0 are the degrees of polymerization at times t and zero, respectively.

On the other hand, the degradation kinetics in a specific acid−base catalysis system can be derived on the basis of a catalytic hydrolysis mechanism (see Scheme 1). According to the above mechanism in acidic buffer, the kinetic law can be set as follows (eq 5):

$$-d[ester]/dt = kK[ester][H^+][H_2O] \quad (5)$$

where $K = [esterH^+]/[ester][H^+]$ and [ester] is the molarity of ester linkages. Since $[H^+]$ in aqueous buffer solution is not changed during the hydrolysis and $[H_2O]$ is present in large excess, eq 5 can simplify to a pseudo-first-order reaction[58] (eq 6):

$$-d[ester]/dt = k_{cat.}[ester] \quad (6)$$

where $k_{cat.} = k_0 + k_H{}^+[H^+] + k_{OH}{}^-[OH^-] = k_0 + k_H{}^+[H^+] + k_{OH}{}^-K_w/[H^+]$ and $K_w = [H^+][OH^-] \simeq 10^{-14}$. Using the relationship between [ester] and M_n:

$$[ester] = \rho(DP - 1)/M_n \quad (7)$$

where ρ is the density of the polymer, integration can lead to eq 8 for the specific acid catalysis system.

$$\ln[(DP - 1)/DP] = -k_{cat.}t + \ln[(DP_0 - 1)/DP_0] \quad (8)$$

The kinetic expression can be also applied in the same way for specific base catalysis system. The average DP at time t is defined in this study as the average repeating number of M_n:

$$DP = (M_n - 18)/58 \quad (9)$$

where 18 is the mass of the end groups and 58 is the mass of PGA repeat unit.

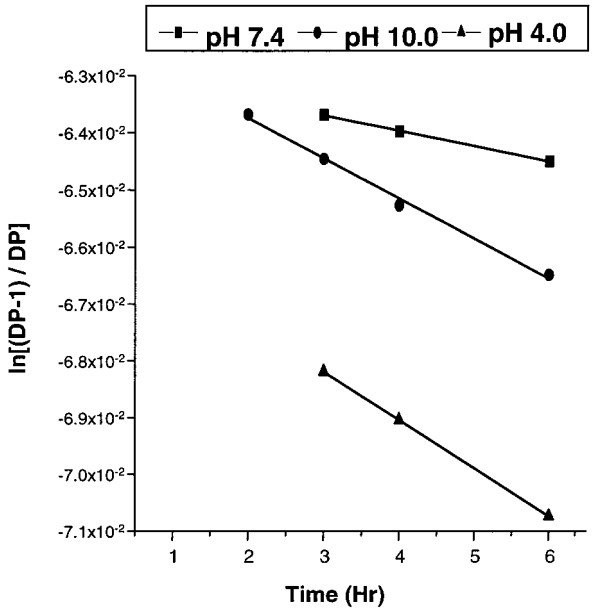

Figure 8. Semilog plots of (DP − 1)/DP vs hydrolysis time for PGA hydrolysis products at the surface in various buffers.

The resulting hydrolytic degradation kinetics at the surface of PGA and semilog plot of (DP − 1)/DP vs hydrolysis time are shown in Table 6 and Figure 8, respectively. Good linearity can be obtained for each treatment condition, and correlation coefficients, R^2, indicate an excellent adherence of the experimental data to the hydrolysis mechanism for PGA from the peak at the 2 or 3 h treatment. The slopes of each line represent hydrolytic degradation rate constants at the surface of PGA. As a result of the kinetics study, the hydrolytic degradation rates in acidic ($k_{cat.} = -8.49 \times 10^{-4}$ h^{-1}) and basic ($k_{cat.} = -7.01 \times 10^{-4}$ h^{-1}) buffers are approximately 3 times faster than that in neutral ISOTON II buffer solution ($k' = -2.67 \times 10^{-4}$ h^{-1}). These results support favorable acid−base catalytic hydrolysis of ester linkages at the surface.

Combined Results from Bulk and Surface Studies. To better understand the relationship between bulk and surface characteristics during the hydrolysis treatment, the hydrolytic degradation kinetics at the surface of PGA have been compared with the corresponding change in crystallinity in the bulk with respect to increasing hydrolysis time. The increase in crystallinity in pH 4.0 sodium biphthalate buffer is less than that in pH 10.0 sodium carbonate buffer, but in both buffer

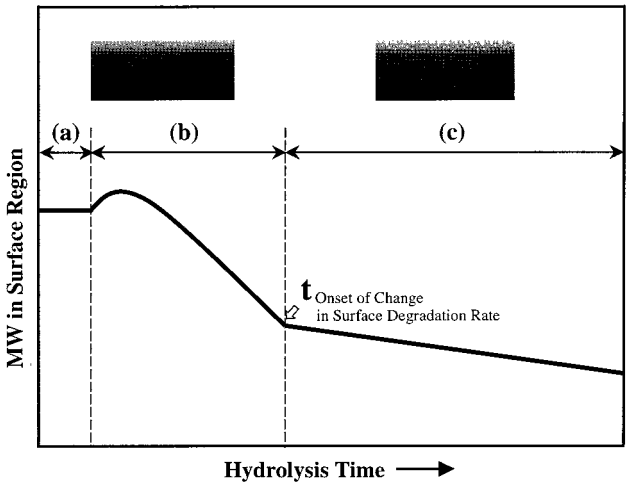

Figure 9. Descriptive MW profile in the surface region of thin (100 μm) PGA films: (a) incubation, (b) onset of abrupt MW change, (c) decrease in surface degradation rate.

media hydrolytic surface degradation rates show almost the same values. As it can be expected in general, carboxylic acid end groups of the hydrolysis products can be present in protonated or dissociated forms both at the surface and in bulk depending on the pH of the buffer media. It has been reported[59,60] that the protonated form of acid groups rendered themselves less hydrophilic and hence less reactive in hydrolysis conditions. So, it can be speculated that in acidic buffer media the hydrolysis products inside of a PGA matrix would become protonated, while in basic buffer they would remain in dissociated form. This speculation is supported by the relatively slower increase in crystallinity as a result of the hydrolysis in pH 4.0 sodium biphthalate buffer solution. The similarity in hydrolytic surface degradation rates in both pH 10.0 and pH 4.0 buffers is explained by the reactions in the surface segregated amorphous region,[17−19] which can be considered as the distinctive surface characteristic at the initial induction stage of hydrolytic erosion process of semicrystalline biodegradable polyesters. A descriptive MW profile in the surface region of thin (100 μm) PGA films can be proposed in Figure 9 which includes (1) the very short incubation (not observed: usually dependent on biodegradable polymers and fabrication methods), (2) the onset of abrupt MW change where the surface segregated amorphous fraction leads to a preferential hydrolytic degradation resulted in the initial increase in MW followed by a decrease, and (3) the decrease[50] in the rate of surface degradation due to the onset of weight loss resulted from the ultimate diffusion of water-soluble hydrolysis products (mainly, monomeric glycolic acid) into external buffers.

Conclusion

The initial "induction" period of hydrolysis at the surface of PGA-based devices is important in drug delivery and the understanding of surface/interface reactions related to inflammation[61,62] in many in vivo applications of biodegradable polyesters. In vitro studies of the hydrolytic degradation of PGA reported in this work present the role of surface amorphous region at the initial stage of erosion profile on surface vs bulk degradation processes in three different pH buffer media. A combination of SEM, XPS, and ToF SIMS provides surface characterization, and DSC and weight loss studies provide results from the bulk phases of the film.

During the first 6 h of exposure no change in weight loss is detectable, yet morphological changes occur at the surface of PGA as observed by SEM. ToF SIMS shows the formation of oligomeric hydrolysis products presumably adsorbed at the surface; these data have been quantified to extract MW of the hydrolysis products and to finally establish the hydrolytic surface degradation kinetics in various pH buffers. The effect of surface degradation on the bulk thermal properties is investigated by comparing ToF SIMS data to the corresponding crystallinity change in the bulk. XPS data show the addition of small amounts of sodium at the surface but no sensitivity to the changes in surface chemistry.

The initial increase of MW followed by a decrease during the induction period is attributed to the preferential degradation of surface segregated amorphous fraction. The hydrolytic degradation rates at the surface of PGA are 3 times faster in both pH 4.0 sodium biphthalate and pH 10 sodium carbonate buffers than that in pH 7.4 physiological electrolyte buffer (ISOTON II).

These results allow three important conclusions about the surface reactivity of PGA-based devices. The surface region is enriched in amorphous PGA more than the interior of the device; thus, the rapid reaction kinetics associated with amorphous polymers dominates the initial reaction period. During the induction period, where few changes in overall device mass may occur, rapid reactions over the top few nanometers predominantly generate short chain polymeric oligomers with very little solubility to the surrounding aqueous phase. Yet, this reactivity could effect a significant initial burst of additives such as drugs being delivered and presumably induce a local decrease in pH. The lower local pH could significantly increase the reaction rate of the surface as acid and base conditions away from physiological pH increase reaction rates. Therefore, the chemistry of the induction period is dominated by surface and interfacial reactions until the equilibration of water penetration and absorption leads to bulk degradation processes. In future work we will extensively examine both surface and bulk characteristics over the hydrolysis time beyond a induction period in order to define the change in hydrolytic surface degradation kinetics due to the onset of weight loss and also the release profile of the soluble fraction using LC/MS.

Acknowledgment. The authors acknowledge support from the National Science Foundation Analytical and Surface Chemistry program, Grants CHE 9704996 and 0079114. We are grateful for the generous donation of materials from Dr. Peter Jarrett of American Cyanamid, Corp.

References and Notes

(1) Langer, R. *MRS Bull.* **1991**, *Sept*, 47.
(2) Kenley, R. A.; Lee, M. O.; Mahoney II, T. R.; Sanders, L. M. *Macromolecules* **1987**, *20*, 2398.
(3) Makino, K.; Ohshima, H.; Kondo, T. *J. Microencaps.* **1986**, *3*, 203.
(4) Pitt, C. G.; Gratzel, M. M.; Kimmel, G. L.; Surles, J.; Schindler, A. *Biomaterials* **1981**, *2*, 215.
(5) Lewis, D. H. In *Biodegradable Polymers as Drug Delivery Systems*; Chasin, M., Langer, R., Eds.; Marcel Dekker: New York, 1990.

(6) Li, S. M.; Garreau, H.; Vert, M. *J. Mater. Sci.: Mater. Med.* **1990**, *1*, 123.
(7) Li, S. M.; Garreau, H.; Vert, M. *J. Mater. Sci.: Mater. Med.* **1990**, *1*, 131.
(8) Therin, M.; Christel, P.; Li, S. M.; Garreau, H.; Vert, M. *Biomaterials* **1992**, *13*, 594.
(9) Davies, M. C.; Short, R. D.; Khan, M. A.; Watts, J. F.; Brown, A.; Eccles, A. J.; Humphrey, P. Vickerman, J. C.; Vert, M. *Surf. Interface Anal.* **1989**, *14*, 115.
(10) Davies, M. C.; Lyyn, R. A. P. *Crit. Rev. Biocompat.* **1990**, *5*, 297.
(11) Davies, M. C.; Khan, M. A.; Short, R. D.; Akhtar, S.; Pouton, C.; Watts, J. F. *Biomaterials* **1990**, *11*, 228.
(12) Shard, A. G.; Volland, C.; Davies, M. C.; Kissel, T. *Macromolecules* **1996**, *29*, 748.
(13) Shard, A. G.; Davies, M. C.; Li, Y. X.; Volland, C.; Kissel, T. *Macromolecules* **1997**, *30*, 3051.
(14) Leadley, S. R.; Davies, M. C.; Vert, M.; Braud, C.; Paul, A. J.; Shard, A. G.; Watts, J. F. *Macromolecules* **1997**, *30*, 6920.
(15) Ivanova, Tz.; Panaiotov, I.; Boury, F.; Proust, J. E.; Benoit, J. P.; Verger, R. *Colloids Surf B: Biointerfaces* **1997**, *8*, 217.
(16) Chen, X.; Shakesheff, K. M.; Davies, M. C.; Heller, J.; Roberts, C. J.; Tendler, S. J. B.; Williams, P. M. *J. Phys. Chem.* **1995**, *99*, 11537.
(17) Allen, A.; Davies, M. C.; Roberts, C. J.; Tendler, S. J. B.; Williams, P. M. *Trends Biotechnol.* **1997**, *15*, 101.
(18) Davies, M. C.; Shakesheff, K. M.; Shard, A. G.; Domb, A.; Roberts, C. J.; Tendler, S. J. B.; Williams, P. M. *Macromolecules* **1996**, *29*, 2205.
(19) Shakesheff, K. M.; Chen, X. Y.; Davies, M. C.; Domb, A.; Roberts, C. J.; Tendler, S. J. B.; Williams, P. M. *Langmuir* **1995**, *11*, 3921.
(20) Frazza, E. J.; Schimitt, E. E. *J. Biomed. Mater. Res. Symp.* **1971**, *1*, 43.
(21) Chujo, K.; Kobayashi, H.; Suzuki, J.; Tokuhara, S. *Makromol. Chem.* **1967**, *100*, 267.
(22) Chatani, Y.; Suehiro, K.; Okita, Y.; Tadokoro, H.; Chujo, K. *Makromol. Chem.* **1968**, *113*, 215.
(23) Gilding, D. K.; Reed, A. M. *Polymer* **1979**, *20*, 1459.
(24) Chujo, K.; Kobayashi, H.; Tokuhara, S.; Tanabe, M. *Makromol. Chem.* **1967**, *100*, 262.
(25) Hirano, H.; Wsai, T.; Saegusa, T.; Furukawa, J. *J. Chem. Soc. Jpn.* **1964**, *67*, 604.
(26) Pitt, C. G.; Schindler, A. In *Controlled Drug Delivery*; Bruck, S. D., Ed.; CRC Press: Boca Raton, FL, 1983.
(27) Leenslag, J. W.; Pennings, A. J.; Bos, R. R. M.; Rozema, F. R.; Boering, G. *Biomaterials* **1987**, *8*, 311.
(28) Kulkarni, R. K.; Pani, K. C.; Neuman, C.; Leonard, F. *J. Biomed. Mater. Res.* **1971**, *5*, 169.
(29) Miller, R. A.; Brady, J. M.; Cutright, D. E. *J. Biomed. Res.* **1977**, *11*, 711.
(30) Jackanicz, T. M.; Nash, H. A.; Wise, D. L.; Gregory, J. *Contraception* **1973**, *8*, 227.
(31) Anderson, L. C.; Wise, D. L.; Howes, J. F. *Contraception* **1976**, *13*, 375.
(32) Wise, D. L.; McCormick, G. J.; Willet, G. P.; Anderson, L. C. *Life Sci.* **1976**, *19*, 867.
(33) Getter, L. Presented at the Fourth Annual Biomaterials Symposium, Clemson University, 1972.
(34) Schmitt, E. E.; Polistina, R. A. U.S. Patent 3297033, 1967.
(35) Schmitt, E. E.; Epstein, M.; Polistina, R. A. U.S. Patent 3422871, 1969.
(36) Glick, A. U.S. Patent 3626948, 1971.
(37) Vainionpaa, S.; Rokkanen, P.; Tormala, P. *Prog. Polym. Sci.* **1989**, *14*, 679.
(38) Williams, D. F. *J. Mater. Sci.* **1982**, *17*, 1233.
(39) *39.Controlled Release of Biologically Active Agents*; Baker, R. W., Ed.; John Wiley & Sons: New York, 1987.
(40) Cooke, T. F. *J. Polym. Eng.* **1990**, *9*, 171.
(41) Reed, A. M.; Gilding, D. K. *Polymer* **1981**, *22*, 494.
(42) Pitt, C. G. In *Biodegradable Polymers and Plastics*; Vert, M., Feijen, J., Albertsson, A., Scott, G., Chiellini, E., Eds.; Royal Society of Chemistry: Cambridge, 1992.
(43) Chu, C. C. *J. Biomed. Mater. Res.* **1981**, *15*, 795.
(44) Ginde, R. M.S. Thesis, State University of New York at Buffalo, 1985.
(45) Dauner, M.; Muller, E.; Wagner, B.; Planck, H. In *Proceedings of 4th International Conference on Degradation Phenomena on Polymeric Materials*; Planck, H., Dauner, M., Renardy, M., Eds.; Springer-Verlag: Berlin, 1992.
(46) Li, S. M.; Vert, M. *Macromolecules* **1994**, *27*, 3107.
(47) Burkhardt, C. A. Ph.D. Dissertation, State University of New York at Buffalo, 1992.
(48) Gardella Jr., J. A.; Hernandez de Gatica, N. L. *J. Electron Spectrosc. Relat. Phenom.* **1996**, *81*, 227.
(49) Chen, J.; Gardella Jr., J. A. *Macromolecules* **1999**, *32*, 7380.
(50) Chen, J.; Lee, J.-W.; Hernandez de Gatica, N. L.; Burkhardt, C. A.; Hercules, D. M.; Gardella Jr., J. A. *Macromolecules* **2000**, *33*, 4726.
(51) Gaur, U.; Lau, S.-F.; Wunderlich, B. B.; Wunderlich, B. *J. Phys. Chem. Ref. Data* **1983**, *12*, 65.
(52) Googly Software, Copyright 1994 Andrew Proctor.
(53) Mathiowitz, E.; Jacob, J.; Pekarek, K.; Chickering III, D. *Macromolecules* **1993**, *26*, 6756.
(54) Lee, J.-W.; Gardella Jr., J. A. *Anal. Chem.*, submitted.
(55) Chawla, A. S.; Chang, T. M. S. *Biomat. Med. Dev., Art. Org.* **1985−86**, *13*, 153.
(56) Coffin, M. D.; McGinity, J. W. *Pharm. Res.* **1992**, *9*, 200.
(57) Zhu, K. J.; Hendren, R. W.; Jensen, K.; Pitt, C. G. *Macromolecules* **1991**, *24*, 1736.
(58) Pitt, C. G.; Chasalow, F. I.; Hibionada, Y. M.; Klimas, D. M.; Schindler, A. *J. Appl. Polym. Sci.* **1981**, *26*, 3779.
(59) Kiss, E.; Vargha-Butler, E. I. *Colloids Surf., B* **1999**, *15*, 181.
(60) Shoichet, M. S.; McCarthy, T. J. *Macromolecules* **1991**, *24*, 982.
(61) Klompmaker, J.; Jansen, H. W. B.; Veth, R. P. H.; de Groot, J. H.; Nijenhuis, A. J.; Pennings, A. J. *Biomaterials* **1991**, *12*, 810.
(62) Böstman, O. M. *Clin. Orthop. Relat. Res.* **1992**, *278*, 193.

MA0022351